Critical and noncritical non-Hermitian topological phase transitions in one-dimensional chains

Rui Aquino, Nei Lopes, and Daniel G. Barci
Departamento de Física Teórica, Universidade do Estado do Rio de Janeiro, Rua São Francisco Xavier 524, 20550-013 Rio de Janeiro, Brazil

(Received 30 August 2022; revised 28 November 2022; accepted 9 January 2023; published 23 January 2023)

In this work we investigate non-Hermitian topological phase transitions using real-space edge states as a paradigmatic tool. We focus on the simplest non-Hermitian variant of the Su-Schrieffer-Heeger model, including a parameter that denotes the degree of non-Hermiticity of the system. We study the behavior of the zero-energy edge states in the nontrivial topological phases with integer and semi-integer topological winding numbers, according to the distance to the critical point. We find that, depending on the parameters of the model, the edge states may penetrate into the bulk, as expected in Hermitian topological phase transitions. We also show that, using the topological characterization of the exceptional points, we can describe the intricate chiral behavior of the edge states across the whole phase diagram. Moreover, we characterize the criticality of the model by determining the correlation length critical exponent directly from numerical calculations of the penetration length of the zero-mode edge states.

DOI: 10.1103/PhysRevB.107.035424

I. INTRODUCTION

Non-Hermitian (NH) Hamiltonians are widely used in effective descriptions of a variety of phenomena. Photonic systems [1–5], semimetals, insulators [6–9], electrical circuits [10,11], and interacting systems [12–18] are some examples in which NH phenomena emerge. One prominent feature of NH Hamiltonians is the appearance of *exceptional points* (EPs) in their spectra [19–21], which arise for specific values of the parameter space. Exceptional points are spectral degeneracies where the eigenvectors coalesce and the NH Hamiltonian becomes defective, inducing remarkable topological properties [22,23] that have been observed and explored in different experimental setups [1–5,9].

NH models exhibit a complex band structure [24], which gives rise to different physical properties when compared to standard Hermitian systems. One example where these differences become evident is the bulk-boundary correspondence. In the Hermitian case, it states that the nonzero winding number ($W \neq 0$) defined in the bulk determines the existence of gapless zero-energy edge states (ZEESs), located at the system's edges (or boundaries). For instance, in the standard Hermitian one-dimensional Su-Schrieffer-Heeger (SSH) model [25] if the winding number is trivial, i.e., $W = 0$, there are no ZEESs, and therefore, the system is a usual insulator. On the other hand, for specific values of the parameters, the system undergoes a topological phase transition. At the latter, the system is known as a topological insulator, where $W = 1$. As a consequence, there will be a pair of ZEESs at the edges of the system (one on the left side and one on the right side of the chain) [26]. In other words, the bulk of the system remains an insulator, while its edges can carry an electric current in the nontrivial topological phase, which makes it so attractive from the technological point of view. By contrast, for NH systems, it is well known that the winding number can be fractionary [27] and that the bulk-boundary correspondence fails [11]. A detailed review, with some attempts to reestablish this correspondence, can be found in Ref. [28].

Although a topological phase transition is essentially discontinuous, in the sense that the winding number jumps discontinuously at the transition, the penetration length of the edge states continuously diverges as a power law with a well-defined exponent. In this sense, at least in the Hermitian case, this kind of transition has *critical* properties [29–31]. Moreover, the interest in the critical properties of NH systems is continuously growing. For instance, analyses of the thermodynamical properties [32] as well as computations of the fidelity susceptibility [33] have been made. Disorder effects have also been investigated [34]. In particular, different works have indicated *directly or indirectly* the importance of the EPs on the criticality of these NH systems [35–37].

In order to contribute to this issue, in this work we analyze an extended SSH model, considering asymmetric hopping [27,32], in order to investigate how the ZEESs behave near topological phase transitions and how they are related to the EPs and their chirality.

By means of numerical calculations, we compute the topological phase diagram, the complex gap structure, and the edge states of the model. Our results show that, depending on the parameters, near the topological transitions, the ZEESs may penetrate into the bulk, as expected from Hermitian topological phase transitions [29–31]. Surprisingly, the ZEESs are not sensitive to the transition from $W = 1/2$ to $W = 1$ winding numbers, which is proper for NH systems. This fact indicates a noncritical character of this particular NH transition. In addition, from the spectrum analysis, we show that one can also characterize the NH topological phase transitions by means of the structure of the complex energy gaps.

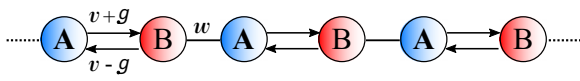

FIG. 1. One-dimensional chain of the non-Hermitian SSH model with asymmetric intracell hopping. Each unitary cell contains a pair of sublattices A and B, the blue and red spheres, respectively. v is the hopping term within the unitary cell, while w is the hopping term out of the unitary cell. The real parameter g measures the degree of non-Hermiticity of the model. When $g = 0$, we recover the standard Hermitian SSH model.

Interestingly, from the topological phase diagram, we find that at the nontrivial topological state with $W = 1$ [dark rhombus in Fig. 4(a) below] the system exhibits two different behaviors for the ZEESs, depending on the parameter space of the model. One of them is essentially equivalent to the usual Hermitian behavior, while the other is proper for NH systems and is known as the NH skin effect [38,39], where the zero-energy modes accumulate on the boundary. Through a careful analysis of the topological characterization of the EPs, which emerge in the spectrum, we describe each one of these edge state behaviors and their chiralities.

Moreover, we characterize the criticality of the system through the identification of the correlation length critical exponent ν of the topological transition from the numerical calculation of the penetration length of the ZEESs as a function of the distance to the topological transition point using concepts of scaling theory and critical phenomena [29,31,40–43].

This paper is organized as follows: In Sec. II we present the NH SSH model including a real parameter that encodes the degree of non-Hermiticity of the system. In Sec. III we describe the topological aspects of the model and characterize the EPs that emerge in NH systems. In Sec. IV we obtain the topological phase diagram and investigate the behaviors of the EPs, ZEESs, and chirality depending on the parameters of the model. In Sec. V we calculate the critical exponents that characterize the NH topological transitions, and consequently, we identify the universality class of the model. Finally, in Sec. VI we conclude and make some remarks about our main results.

II. THE SSH MODEL WITH ASYMMETRIC HOPPING

We will analyze the simplest NH variant of the one-dimensional SSH model. In this modified version of the SSH model, we introduce a real parameter g, which denotes an asymmetry in the intracell hopping v. As usual, there is also a term that encodes the intercell hopping w. In Fig. 1 we show a schematic representation of the one-dimensional chain of the non-Hermitian SSH model.

The Hamiltonian reads [27,32]

$$H = \sum_n [(v-g)a_n^\dagger b_n + (v+g)b_n^\dagger a_n + w(a_{n+1}^\dagger b_n + b_n^\dagger a_{n+1})], \tag{1}$$

where $a_n^\dagger$ (a_n) and $b_n^\dagger$ (b_n) are the creation (annihilation) operators at the nth A and B sites, respectively. Note that the parameter g acts as the degree of non-Hermiticity of the system, and when $g = 0$, we recover the SSH model [25].

Performing a Fourier transformation and using $\psi = (b_k, a_k)^T$, we can rewrite the Hamiltonian in Eq. (1) as follows:

$$H = \sum_k \psi_k^\dagger h(k) \psi_k, \tag{2}$$

with the one-particle Hamiltonian in the form

$$h(k) = h_x(k)\sigma_x + h_y(k)\sigma_y, \tag{3}$$

where $\sigma_{x,y}$ are the Pauli matrices and the components h_x and h_y are given by [27,32]

$$h_x(k) = v + w\cos(k), \tag{4}$$

$$h_y(k) = w\sin(k) - ig. \tag{5}$$

For simplicity, we measure distances in terms of the lattice spacing a, or we simply set $a = 1.0$. Note, again, that if $g = 0$, we recover the Hermitian SSH model [25], as expected. Due to the fact that $v, w \in \mathbb{R}$, explicitly putting Eqs. (4) and (5) into Eq. (3), one can see how the parameter g breaks the Hermiticity of the Hamiltonian. Computing the dispersion relation of Eq. (3), we find $E_\pm = \pm\sqrt{h_x^2 + h_y^2}$, as usual.

When dealing with Hermitian systems, Hermiticity ensures real eigenvalues as well as orthogonal eigenvectors. On the other hand, for NH systems the eigenvalues may be complex, and the Hamiltonian allows a complete biorthonormal system of eigenvectors when it is diagonalizable [44]. In conclusion, the Hilbert space of the system supports a biorthogonal basis $\langle u_\pm | \tilde{u}_\pm \rangle = \delta_{ij}$, where $i, j = +, -$ and $\tilde{u}$ is the dual of u. These bases are defined by

$$h(k)|u_\pm\rangle = E(k)|u_\pm\rangle, \tag{6}$$

$$h^\dagger(k)|\tilde{u}_\pm\rangle = E^*(k)|\tilde{u}_\pm\rangle, \tag{7}$$

where the eigenvectors are given by

$$|u_\pm\rangle = \begin{pmatrix} \pm e^{-i\phi(k)} \\ 1 \end{pmatrix}, \quad |\tilde{u}_\pm\rangle = \begin{pmatrix} \pm e^{-i\phi^*(k)} \\ 1 \end{pmatrix} \tag{8}$$

and

$$\phi(k) = \tan^{-1}\left(\frac{h_y}{h_x}\right). \tag{9}$$

Note that $h_y(k)$ is a complex function that depends on k [see Eq. (5)]. So the angle $\phi(k)$ in Eq. (9) is, in general, complex.

It is worth emphasizing that due to the complex character of the dispersion relation $E(k)$, the spectrum has a more involved structure than in the Hermitian case. So when dealing with NH systems, we have two independent definitions of complex energy gaps, which are given by the following statements [7]:

(i) *Point gap.* A NH system presents a point gap if and only if it is invertible and has nonzero eigenenergies, i.e., $\det H(k) \neq 0$ and $E(k) \neq 0\,\forall\, k$, respectively.

(ii) *Real (imaginary) line gap.* A NH system presents a line gap in the real (imaginary) part of its spectrum if and only if it is invertible and the real (imaginary) part of the

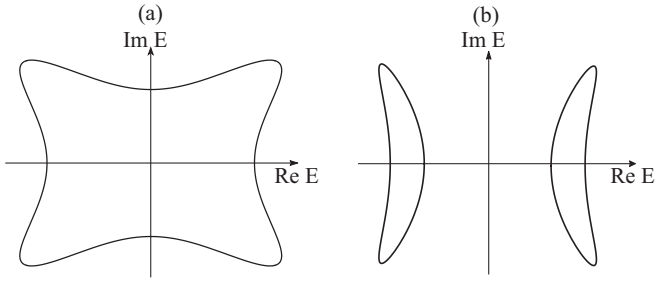

FIG. 2. (a) The complex energy gap for $v = 0.3$ and $g = 1.0$. For these parameters we have a point gap spectrum. (b) The complex real line gap for $v = -0.1$ and $g = 0.6$. We fix $w = 1.0$ in both panels.

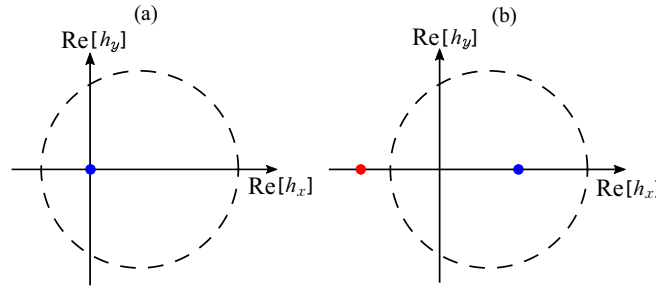

FIG. 3. $\{\mathrm{Re}[h_x], \mathrm{Re}[h_y]\}$ plane and the encircling (dashed circles) of the exceptional points (red and blue dots) with fixed $w = 1.0$. (a) We take $g = 0$ and $v = 0.5$, i.e., the nontrivial topological phase of the standard Hermitian SSH model with $W = 1$. (b) Non-Hermitian topological phase with $W = 1/2$, where $g = 0.8$ and $v = 0.5$. Note that in the Hermitian case both exceptional points are located at the origin, while in the non-Hermitian case the exceptional points are shifted along the $\mathrm{Re}[h_x]$ axis, and only one is encircled.

eigenenergies is nonzero, i.e., $\det H(k) \neq 0$ and $\mathrm{Re}E(k) \neq 0$ ($\mathrm{Im}E(k) \neq 0$) $\forall\, k$, respectively.

The structure of the complex energy gaps is extremely important to the topological characterization of NH systems, as we will discuss later. In Fig. 2 we plot some examples of gaps that appear in the NH SSH model with asymmetrical hopping, and in Sec. IV we will give more details about the complex energy gaps through the topological phase diagram of the model.

III. TOPOLOGY AND EXCEPTIONAL POINTS

In the usual tenfold classification of Hermitian topological phases [45,46], three symmetries are required for its description, which are the time-reversal, particle-hole, and chiral symmetries. On the other hand, in the NH classification [47], symmetries ramify due to the distinction between transposition and complex conjugation in NH Hamiltonians. In fact, chiral symmetry, which gives rise to the topological properties of the Hermitian SSH model, is distinct from the sublattice symmetry, although they are equivalent in Hermitian physics. The NH SSH model, defined in the last section, belongs to class A with an additional sublattice symmetry (SLS), as defined in [7],

$$\mathcal{S}h(k)\mathcal{S}^{-1} = -h(k), \quad \mathcal{S}^2 = 1, \tag{10}$$

where $\mathcal{S}$, in general, is a unitary matrix of the non-Hermitian 38-fold classification (note that the model does not have chiral symmetry, so it does not respect any $AZ^\dagger$ symmetry).

For the Hamiltonian given by Eq. (3), $\mathcal{S} := \sigma_z$. Additionally, we have the winding number defined as [27]

$$W = \frac{1}{2\pi}\oint \partial_k \phi \, dk, \tag{11}$$

where ϕ was previously defined in Eq. (9) and the integral is taken along a loop with k from 0 to 2π.

It is interesting to point out that if we compute the winding number for the Hamiltonian in Eq. (3), we find that W is quantized as $\mathbb{Z}/2$, rather than $\mathbb{Z}$, as we have in the Hermitian SSH model. This fractional winding number, although unexpected, is in agreement with other topological characterizations of NH systems. In Ref. [7], class A with SLS defines a $\mathbb{Z}$ winding number for systems with a line gap spectrum and a $\mathbb{Z} \oplus \mathbb{Z}$ winding number for a point gap spectrum (see Table VI of Ref. [7]). As pointed out in Ref. [27], we can rearrange Eq. (11) as $2W = W_1 + W_2$, where W_1 and W_2 are $\mathbb{Z}$ topological invariants, so we can recover all the results of the topological characterization of Ref. [7] using W_1 and W_2 as defined in Ref. [27]. Interestingly, this $\mathbb{Z}/2$ winding number was recently realized in quantum simulators [9].

Due to the fact that Eq. (11) has contributions from only the real part of the angle $\phi(k)$, we can geometrically interpret the $\mathbb{Z}/2$ quantization as the manifestation of the encircling of the EPs of the model in the $\{\mathrm{Re}[h_x], \mathrm{Re}[h_y]\}$ space. To understand this, let us find the location of the EPs by computing the zeros of the dispersion relation, i.e., $h_x^2 + h_y^2 = 0$, or, equivalently,

$$\mathrm{Re}[h_x] = -\mathrm{Im}[h_y], \quad \mathrm{Re}[h_y] = \mathrm{Im}[h_x], \tag{12}$$

$$\mathrm{Re}[h_x] = \mathrm{Im}[h_y], \quad \mathrm{Re}[h_y] = -\mathrm{Im}[h_x]. \tag{13}$$

So we can conclude that each of the two EPs appears in the ordered pairs $(-\mathrm{Im}[h_y], \mathrm{Im}[h_x])$ and $(\mathrm{Im}[h_y], -\mathrm{Im}[h_x])$. In Fig. 3 we show some examples of the different phases of the model described by the EPs. In Fig. 3, the dashed circles are the geometrical points of $(\mathrm{Re}[h_y(k)], \mathrm{Re}[h_x(k)])$ when k goes from 0 to 2π for fixed values of the parameters.

In Fig. 3(a) we have both EPs merging at the origin, that is, $(h_x, h_y) = (0, 0)$, which can be recognized as the nontrivial topological phase of the usual Hermitian SSH model with $W = 1$, while in Fig. 3(b) we have an exclusive NH topological phase where $W = 1/2$. Note that for the latter, only one EP is encircled.

In general, we can conclude that when two EPs are encircled, $W = 1/2$. On the other hand, when only one of them is wound, $W = 1/2$. Finally, when no EPs are encircled, $W = 0$. We will use the trajectories of the EPs to describe the chirality and the phase transitions of the model.

IV. TOPOLOGICAL PHASE DIAGRAM, CHIRALITY, AND EDGE STATES

The topological phase diagram of the NH SSH model can be obtained through the calculation of the topologically invariant winding number given by Eq. (11). The phases that emerge in the model are characterized by $W = 0, 1/2$, and 1, as shown in Fig. 4(a). The central dark rhombus is characterized by a

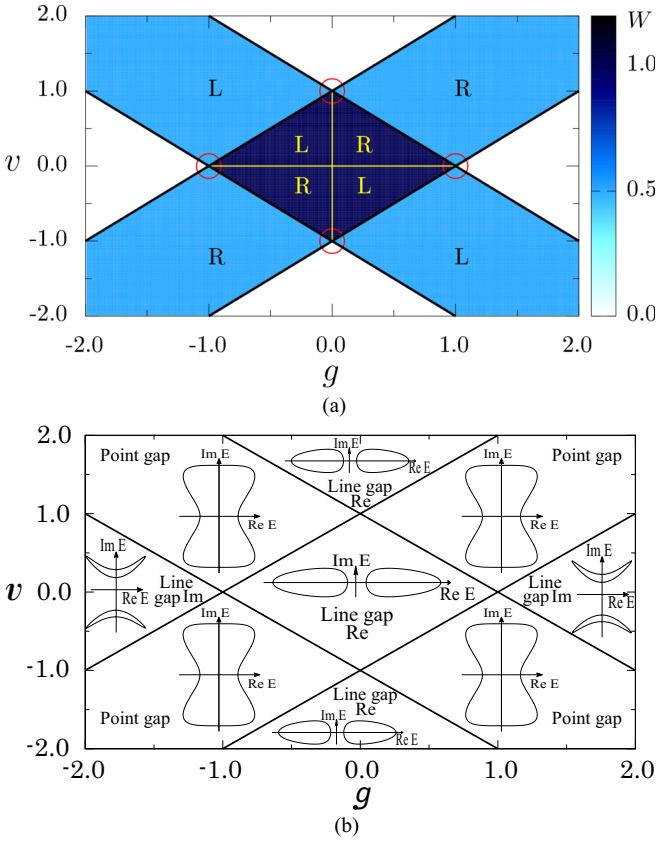

FIG. 4. (a) Phase diagram of the non-Hermitian SSH model obtained from the calculation of Eq. (11) with fixed $w = 1.0$. We can see three topological phases characterized by $W = 0$, $1/2$, and 1 (see color bar). The chirality of the model is represented by the presence of left (L) or right (R) zero-energy edge states. Within the vertical and horizontal solid yellow lines there are edge states on both sides (left and right) of the chain, and they penetrate into the bulk of the system as we approach the transition point. Note that these solid lines divide the phase diagram into four quadrants inside the rhombus with $W = 1$, where the chirality depends on the parameters of the model even at the nontrivial topological state with an integer topological winding number. (b) Complex gap structure in each phase of the system.

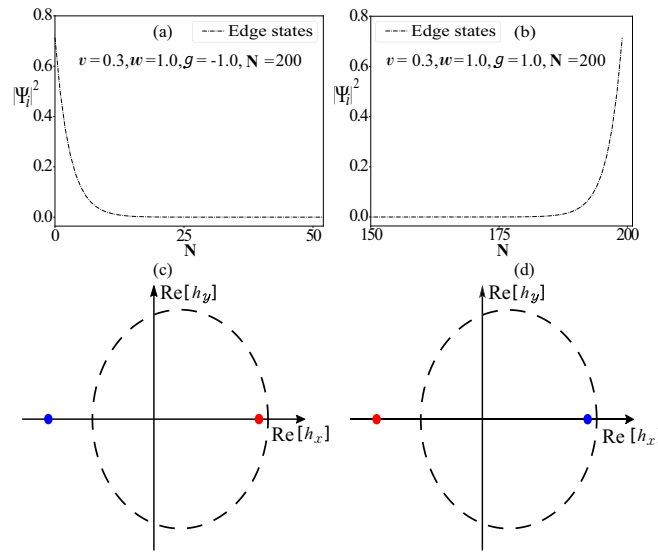

FIG. 5. Chirality of the zero-energy edge states as we enter the fractional topological phase with $W = 1/2$ from the trivial one. (a) Left edge states in the semi-integer topological phase with left chirality. (b) Right edge states in the semi-integer topological phase with right chirality. (c) The left chirality can be determined by the EP (red dot) that first enters the dashed unit circle, which is in the $\{\mathrm{Im}[h_y], -\mathrm{Im}[h_x]\}$ position. (d) The right chirality can be determined by the EP (blue dot) that first enters the dashed unit circle, which is in the $\{-\mathrm{Im}[h_y], \mathrm{Im}[h_x]\}$ position. In (c) and (d) we fix $v = 0.3$ and take $g = -1.2$ and $g = 1.2$, respectively. We show a restricted region of the chain in (a) and (b) since there are only left or right edge states.

winding number $W = 1$; the blue zones out of the rhombus are characterized by $W = 1/2$, while the white zones are in the trivial topological phase $W = 0$. On the other hand, in Fig. 4(b) we depict the complex gap structure of the model. Note that the central rhombus exhibits a real line gap, while the phases with a fractional winding number present a point gap. Interestingly, the $W = 0$ regions have two different line gaps. The upper and lower trivial regions ($W = 0$) have a real line gap, while the left and right $W = 0$ regions have imaginary line gaps.

Moreover, also note from Fig. 4(b) that within the line $g = 0$, i.e., in the Hermitian case, the topological phase transitions exhibit only the real line gap, as expected. However, when dealing with NH systems, i.e., for $g \neq 0$, one can see that when the NH system undergoes a topological phase transition, the gap structure necessarily changes. Thus, we can also characterize the NH system through its complex gap structure.

In the following we will discuss the chiral aspects of the topological phase diagrams presented in Fig. 4(a) and the character of the ZEESs as we approach the NH topological phase transitions.

A. Chirality

In the topologically trivial phase with $W = 0$ the system does not have ZEESs and behaves as a conventional insulator, as expected. In the exclusive NH topological phase, where $W = 1/2$, the two ZEESs are accumulated at the edge (left or right side) of the chain, which is a direct manifestation of the NH skin effect [28,38]. Moreover, the accumulation of the ZEESs respects the chirality depicted in Fig. 4(a). This behavior has a direct relation to the EPs and its position in the $\{\mathrm{Re}[h_x], \mathrm{Re}[h_y]\}$ space.

The chirality of the ZEESs is determined by which EP enters the unit circle first. For instance, in the topological phase diagram in Fig. 4(a) the fractional phases with left or right chirality exhibit left or right ZEESs, respectively [see Figs. 5(a) and 5(b)]. In Fig. 5(c) we show that the EP in the position $\{\mathrm{Im}[h_y], -\mathrm{Im}[h_x]\}$ (red dot in all the figures) enters the dashed unit circle first as we approach the semi-integer topological phase with left chirality from the trivial one, while Fig. 5(d) shows that the EP in position $\{-\mathrm{Im}[h_y], \mathrm{Im}[h_x]\}$ (blue dots in all the figures) enters in the dashed unit circle first as we approach the semi-integer topological phase with right chirality from the trivial one.

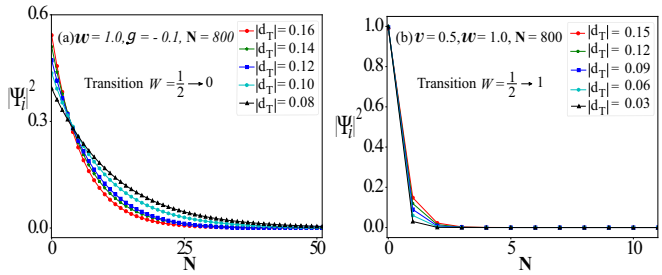

FIG. 6. Penetration of the zero-energy edge states as we approach the topological transition point while varying v and g, respectively. (a) The edge states penetrate into the bulk from the semi-integer to trivial topological transition. (b) The edge states get more localized for the semi-integer to integer transition as we approach the criticality, increasing the degree of non-Hermiticity of the system. Again, we show only part of the chain on the x axis since we just have edge states on the left side. d_T is the distance to the transition point.

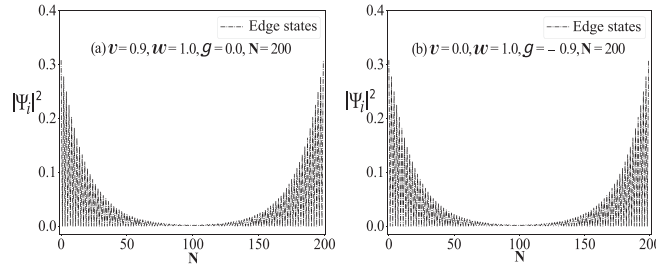

FIG. 7. Exponential decay of the amplitude of the wave function of the zero-energy edge modes into the bulk according to the phase diagrams in Fig. 4. (a) and (b) Edge state decay for vertical and horizontal solid lines taking $g = 0.0$ and $v = 0.0$ close to the transition point, respectively.

Surprisingly, the topological phase transition from $W = 1/2$ to $W = 1$, and vice versa, does not affect the chirality of the edge states, as can be seen in Fig. 4(a). This indicates an odd character of this transition, which will be explored in the discussion of the ZEES behavior in the next section. Moreover, inside the rhombus with $W = 1$, we find an interesting behavior for the chirality of the ZEESs. When we cross the $g = 0$ line, the chiralities of the ZEES change. This can be understood by the shift of the EPs around the origin of the $\{\mathrm{Re}[h_x], \mathrm{Re}[h_y]\}$ space. Within this line, we have the Hermitian SSH model [25], so this crossover passing through the Hermitian limit of the model affects the chirality. Analogously, if we cross the $v = 0$ line, we also have a change in the chirality. We can track this through the symmetry that the model has in the "parity" transformation of the parameters $(v, g) \rightarrow (-v, -g)$. In fact, the EP positions are the same if we perform this change in the parameters.

The chiral behavior of the ZEESs in the fractional phase was previously reported in Ref. [27], but we clarify the two lines for $g = 0.0$ and $v = 0.0$ inside the rhombus with $W = 1$ and the relation of the chirality in this region to the EPs.

B. Edge states and exceptional points

When we approach the transition with $W = 1/2 \rightarrow W = 0$, i.e., the semi-integer to trivial topological phase transition, the ZEESs penetrate into the bulk in the same sense as Hermitian topological phase transitions [29,31] [see Fig. 6(a)]. By contrast, when we approach the topological phase transition with $W = 1/2 \rightarrow W = 1$, we obtain distinct behaviors as we approach the transition point. For instance, the ZEESs get more localized on the left (or right) side of the system as we approach the transition point, increasing the degree of non-Hermiticity g [see Fig. 6(b)]. On the other hand, as we approach the transition while decreasing the value of g, the ZEESs tend to penetrate into the bulk (not shown). In this sense, we confirm that the degree of non-Hermiticity of the system is associated with the chirality and acts to localize the ZEES at the edges of the system. Furthermore, the ZEES are not affected if we approach the semi-integer to integer topological transition and vice versa, considering the same angular coefficient for the chiral regions as in the topological phase diagram in Fig. 4(a) (not shown), which, again, suggests an unusual aspect for the NH topological transitions. In the next section, we will relate the nonunique character of this phase transition to a noncritical behavior. However, note that we can, indeed, identify all the topological phase transitions of the model through the change in the complex spectrum structure, as pointed out before [see Fig. 4(b)].

Let us now focus on the rhombus with $W = 1$. Note that the solid vertical line for $g = 0$ in Fig. 4(a) recovers the usual topological transitions presented in the Hermitian SSH model [25,29]. The ZEES on this line, near the transition, at the upper edge of the rhombus, is shown in Fig. 7(a). The edge states and the transition for the bottom edge of the rhombus are completely symmetric, i.e., changing the sign of $v \rightarrow -v$, as suggested by the topological phase diagram.

Surprisingly, on the horizontal solid line in Fig. 4(a), i.e., for $v = 0$, at the nontrivial topological phase with $W = 1$ we also obtain ZEESs at the both edges of the chain, as shown in Fig. 7(b). This kind of behavior for the exclusive anti-Hermitian case can be understood from the Hamiltonian in Eq. (1). Note that when $v = 0$, the hopping terms present the same magnitude in the modulus, i.e., $|g|$, which implies that the net particle flux is equal for both sides (left and right) of the chain. These two ZEESs are completely symmetric, and the edge states penetrate into the bulk as we approach the topological transition.

This penetration is expected for $g = 0.0$, that is, for the Hermitian case, but it is not so trivial for the horizontal line where $v = 0.0$. In this limit, the unit cell is completely anti-Hermitian; however, clearly its edge states behave exactly as the full Hermitian limit of the NH SSH model. If we investigate the trajectories of the EPs in the $\{\mathrm{Re}[h_x], \mathrm{Re}[h_y]\}$ parameter space, we see that, due to the fact that $v = 0.0$, the unit circle is fixed at the origin, and the trajectories of the EPs are perfectly symmetric with respect to the circle. For the phases with $v \neq 0.0$ and $g \neq 0.0$, the asymmetry of the trajectories induces topological phase transitions where one EP at a time enters the unit circle. This is not the case for $v = 0.0$; that is, when we approach the topological phase transitions at $g = -1.0$ and $g = 1.0$, the EPs cross the unit circle together. Another interesting point is that the gaps within the line $v = 0.0$ change from imaginary to real line

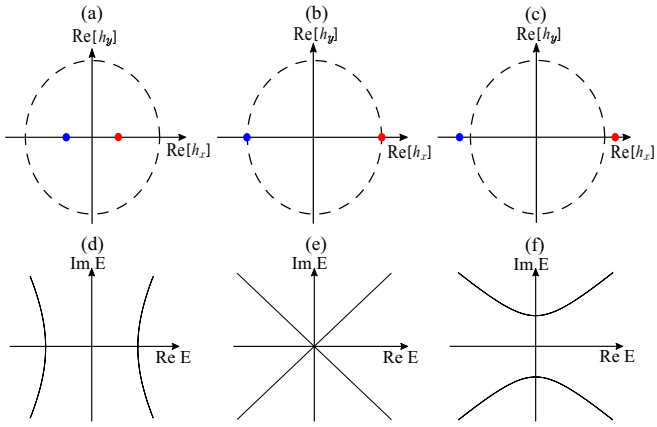

FIG. 8. (a)–(c) The $\{\mathrm{Re}[h_x], \mathrm{Re}[h_y]\}$ parameter space as we approach the topological transition within the horizontal solid line with fixed $v = 0.0$ in Fig. 4(a) for $g = -0.6$, $g = -1.0$, and $g = -1.1$, respectively. The dashed unit circle remains fixed at the origin, while the exceptional points move along the x axis. For this case, both exceptional points enter ($W = 1$) or leave ($W = 0$) the unit circle together at the topological transition point. (d)–(f) The line gaps for the same values of g as in (a)–(c), respectively, showing the nontriviality of these topological phase transitions within this special line.

gaps (and vice versa) at the topological phase transitions [see Fig. 4(b)]. In this special limit, the edge modes behave exactly as in a Hermitian topological phase transition. We show these trajectories of the EPs and their complex gaps in Fig. 8.

On the other hand, for any other case outside the solid vertical or horizontal line in the region with $W = 1$ in Fig. 4, we recover the NH skin effect, with the two modes accumulating on the left or right edges. In this sense, we can conclude that the two vertical and horizontal lines divide the rhombus where $W = 1$ into four quadrants. Again, these results are completely symmetric for even and odd quadrants.

V. TOPOLOGICAL SURFACE STATES AND CRITICAL EXPONENTS

When a system undergoes a phase transition, in principle, there is only one diverging length, i.e., the correlation length ξ, that dominates the phase transition in proximity to the quantum critical point. Our main goal, when applying the penetration depth technique [29,31], is to identify the diverging behavior of the penetration depth of the zero-energy edge modes into the bulk as we approach the topological transition point.

It is possible to get information about the critical exponents from simple scaling assumptions. For instance, very near the phase transition, the singular term of the ground state energy density scales as $f_s \propto |t - t_c|^{\nu(d+z)}$, where t is a generic control parameter and t_c is the transition point. d is the dimensionality of the system, z is the dynamical critical exponent, and the critical exponent ν characterizes the divergence of the correlation length [30]. Moreover, in the one-dimensional non-Hermitian SSH case, the modulus of the spectrum of excitations very close to the topological phase transition can be written as

$$|E(k)| \sim \sqrt{|t - t_c|^{2\nu z} + k^{2z}}. \tag{14}$$

As an example, let us consider, for instance, $v = 0$ and $g \to 1$ in our model. In this case, by direct calculation,

$$|E(k)| \sim \sqrt{2}\{(1 - g)^2 + k^2\}^{1/4}. \tag{15}$$

Thus, $\lim_{g\to 1} |E(k)| \sim k^{1/2}$, and $\lim_{k\to 0} |E(k)| \sim (1 - g)^{1/2}$. Comparing Eq. (15) with Eq. (14), we identify $2z = 1$ and $2\nu z = 1$. Therefore, we get $\nu = 1$. We have checked all the transition lines of our model, obtaining $\nu = 1$ for all the transitions from a nontrivial winding to a trivial one.

In this section, we will confirm the scaling hypothesis by direct numerical calculation of the edge states in real space. Since we already know the critical parameters, given exactly in Fig. 4(a), instead of a finite-size scaling technique [48], we choose an equivalent numerical procedure that has lower computational cost and has already proved to be very accurate in similar cases [29–31]. In this sense, diagonalizing numerically the Hamiltonian given by Eq. (1), in real space, one can obtain the eigenvalues and eigenvectors for the one-dimensional chain with N sites. To define the penetration depth as the diverging length of the topological transition, in principle, the ZEESs may penetrate into the bulk as we approach the transition point. In addition, we consider the distance to the transition point in the form $d_T = |t - t_c|$, where t is a generic control parameter and t_c is the transition point. Since the wave function of the zero-energy edge modes decays exponentially as we approach the topological transition point, we can identify the correlation length ξ as the diverging length of the topological transition, and therefore, we can use the scaling relation $\xi \propto |t - t_c|^{-\nu}$ to obtain the value of the correlation length critical exponent ν by means of a log vs log plot [29,31], as shown in Fig. 9.

Following this procedure, we can investigate the topological phase diagrams of the non-Hermitian SSH model, given by Fig. 4, in order to calculate the values of ν for the topological transitions and, consequently, characterize the criticality of the SSH model with asymmetric hopping. We calculate the value of the critical exponent ν for the topological transition points at the edges of the rhombus with $W = 1$ [see red circles in Fig. 4(a)]. We approach the topological transition points from different paths described by the superscript arrows in Table I, and our numerical results show that these zero-energy edge states penetrate into the bulk, which makes the penetration depth method [29,31] suitable. Note that all values of ν are very close to unity, meaning that even for NH topological transitions, the universality class of the system is the same as that for the Hermitian SSH model for the topological transitions at the edges of the rhombus with $W = 1$.

On the other hand, for the transition within the diagonals of the rhombus with $W = 1$, i.e., for the integer/semi-integer topological transitions and vice versa, the ZEESs exhibit distinct behaviors depending on the approach to the transition point. For example, if we approach the transition point while fixing the value of v and increasing the degree of non-Hermiticity of the system, the ZEESs localize at the edges (left or right side) of the system due to the NH skin effect [28,38], which is very similar to the behavior presented in Fig. 6(b).

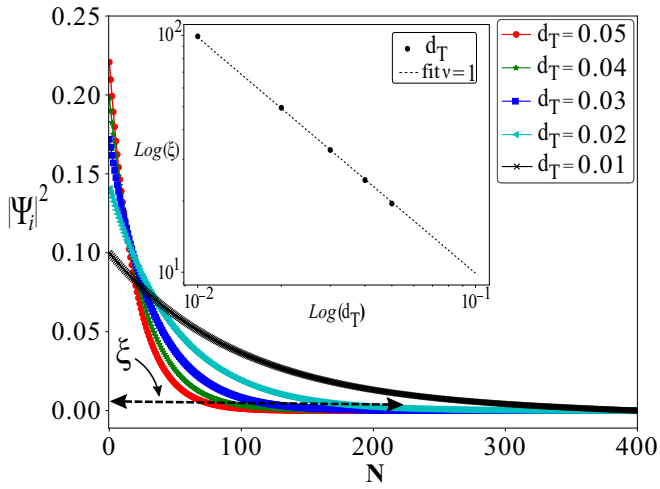

FIG. 9. Exponential decay of the wave function of the zero-energy edge modes into the bulk of the system for the one-dimensional SSH model with $N = 800$ and fixed $w = 1.0$ and $g = 0.0$, where $d_T = |t - t_c|$, as we approach the transition point. Note that the edge states penetrate into the bulk as we get closer to the critical point ($\xi \to \infty$). Defining ξ as the correlation length of the topological transition and using the scaling relation $\xi \propto d_T^{-\nu}$, we can identify the correlation length critical exponent $\nu = 1$ by means of the angular coefficient of the fitting curve in a log vs log plot (see the inset).

By contrast, if we approach the transition point while fixing v and decreasing the value of g, the ZEESs tend to slightly penetrate into the bulk, which confirms that the degree of non-Hermiticity of the system plays an important role in localizing the ZEESs at the edges (left or right side). Furthermore, if we approach the integer/semi-integer transitions along the left or right chiral region while taking the same angular coefficient of the chiral lines as in the topological phase diagram, the ZEESs are not affected, which denotes a noncritical feature for these types of NH topological transitions due to the fact that there is no diverging correlation length in this transition.

TABLE I. Critical points, winding numbers, and the correlation length critical exponents ν obtained by means of the penetration depth technique with $N = 800$ for the edges of the rhombus (red circles) with $W = 1$ in the topological phase diagram given in Fig. 4(a). ν_h (horizontal approach) and ν_v (vertical approach) as well as the superscript arrows describe different forms of approaching the transition point. We observe that all values of ν are very close to unity.

(v, g)	W	ν
(0.95,0.0)	1	$\nu_v^{\uparrow} = 0.998$
(−0.95, 0.0)	1	$\nu_v^{\downarrow} = 0.998$
(0.0,0.95)	1	$\nu_h^{\rightarrow} = 0.998$
(0.0, −0.95)	1	$\nu_h^{\leftarrow} = 0.998$
(1.0, −0.15)	1/2	$\nu_h^{\rightarrow} = 0.979$
(0.23, −1.0)	1/2	$\nu_v^{\downarrow} = 0.944$
(−1.0, 0.15)	1/2	$\nu_h^{\leftarrow} = 0.979$
(−0.23, 1.0)	1/2	$\nu_v^{\uparrow} = 0.944$

VI. SUMMARY AND DISCUSSION

We have studied the NH topological phase transitions of the SSH model with asymmetric hopping using numerical methods to compute the edge states and an analytical approach to display the topological characterization of the exceptional points. One of our main results is shown in Fig. 4. We computed in detail the numerical ZEESs and defined their nontrivial chirality in the rhombus with winding $W = 1$. In particular, the line where $v = 0.0$ presents a Hermitian behavior due to the lack of the NH skin effect; that is, each mode is on a specific edge of the system, and at the topological phase transitions, for $g = -1.0$ and $g = 1.0$, the modes penetrate into the bulk. We used the flow of the exceptional points in the $\{\mathrm{Re}[h_x], \mathrm{Re}[h_y]\}$ space to describe the chiral behavior in the entire rhombus.

We also confirmed that the degree of non-Hermiticity of the NH systems is related to the skin effect [28,38] that localizes the edge states at the boundary (left of right side) of the system. Our numerical results show that the semi-integer/integer topological transition and the reverse present an unusual aspect of the edge states; that is, depending on the direction in parameter space from which the transition point is approached, the edge states may localize or might slightly penetrate into the bulk. Interestingly, when the transition point is approached considering the same angular coefficient as that of the chiral lines of the topological phase diagram, these edge states are invariant on both sides of the transition. Thus, the transition from $W = 1/2$ to $W = 1$ (or vice versa) is not critical, and the edge states remain equally localized on each side of the transition in the phase diagram.

From the complex gap structure analysis we confirm that for the Hermitian case, i.e., for $g = 0.0$, the spectrum of the system does not change when the system undergoes a topological phase transition, exhibiting the real line gap, as expected. On the other hand, when we consider NH effects, that is, for $g \neq 0.0$, we show that one can identify all the NH topological phase transitions on the NH SSH model by the change in its spectrum.

Moreover, applying the penetration depth technique [29,31,40], we have obtained the critical exponent ν for the topological phase transitions at the vertex of the rhombus with $W = 1$ and on the transition lines $W = 1/2 \to 0$ in the topological phase diagram of the NH SSH model. Our results show that the universality class of the NH SSH model is the same as that of the Hermitian SSH model for these specific transition points.

It would be interesting to investigate the model in the limit $v \to 0$, where we have Hermitian topological phase transitions even though the system is non-Hermitian. Also the integer/semi-integer phase transition still represents a challenge. So these aspects might be an interesting direction for further investigations.

ACKNOWLEDGMENTS

The Brazilian agencies Fundação Carlos Chagas Filho de Amparo à Pesquisa do Estado do Rio de Janeiro (FAPERJ), Conselho Nacional de Desenvolvimento Científico e Tecnológico (CNPq), and Coordenação de Aperfeiçoamento de Pessoal de Nível Superior (CAPES), Finance Code 001,

are acknowledged for partial financial support. R.A. would like to thank FAPERJ for his current Ph.D. fellowship. N.L. would like to thank the FAPERJ for the postdoctoral fellowship of the Programa de Pós-Doutorado Nota 10-2020 (E-26/202.184/2020) as well as for the Bolsa de Bancada para Projetos (E-26/202.185/2020).

[1] S.-B. Lee, J. Yang, S. Moon, S.-Y. Lee, J.-B. Shim, S. W. Kim, J.-H. Lee, and K. An, Phys. Rev. Lett. **103**, 134101 (2009).
[2] H. Xu, D. Mason, L. Jiang, and J. G. E. Harris, Nature (London) **537**, 80 (2016).
[3] J. Doppler, A. A. Mailybaev, J. Böhm, U. Kuhl, A. Girschik, F. Libisch, T. J. Milburn, P. Rabl, N. Moiseyev, and S. Rotter, Nature (London) **537**, 76 (2016).
[4] C. Hahn, Y. Choi, J. W. Yoon, S. H. Song, C. H. Oh, and P. Berini, Nat. Commun. **7**, 12201 (2016).
[5] W. Chen, Ş. Kaya Özdemir, G. Zhao, J. Wiersig, and L. Yang, Nature (London) **548**, 192 (2017).
[6] Y. Xu, S.-T. Wang, and L.-M. Duan, Phys. Rev. Lett. **118**, 045701 (2017).
[7] K. Kawabata, K. Shiozaki, M. Ueda, and M. Sato, Phys. Rev. X **9**, 041015 (2019).
[8] A. A. Zyuzin and A. Y. Zyuzin, Phys. Rev. B **97**, 041203(R) (2018).
[9] W. Zhang, X. Ouyang, X. Huang, X. Wang, H. Zhang, Y. Yu, X. Chang, Y. Liu, D.-L. Deng, and L.-M. Duan, Phys. Rev. Lett. **127**, 090501 (2021).
[10] T. Yoshida, T. Mizoguchi, and Y. Hatsugai, Phys. Rev. Res. **2**, 022062(R) (2020).
[11] T. Helbig, T. Hofmann, S. Imhof, M. Abdelghany, T. Kiessling, L. W. Molenkamp, C. H. Lee, A. Szameit, M. Greiter, and R. Thomale, Nat. Phys. **16**, 747 (2020).
[12] Y. Michishita, T. Yoshida, and R. Peters, Phys. Rev. B **101**, 085122 (2020).
[13] V. Kozii and L. Fu, arXiv:1708.05841 (2017).
[14] J. A. S. Lourenço, R. L. Eneias, and R. G. Pereira, Phys. Rev. B **98**, 085126 (2018).
[15] T. Yoshida, R. Peters, and N. Kawakami, Phys. Rev. B **98**, 035141 (2018).
[16] T. Yoshida, R. Peters, N. Kawakami, and Y. Hatsugai, Phys. Rev. B **99**, 121101(R) (2019).
[17] R. Aquino and D. G. Barci, Phys. Rev. B **102**, 201110(R) (2020).
[18] R. Schäfer, J. C. Budich, and D. J. Luitz, Phys. Rev. Res. **4**, 033181 (2022).
[19] I. Rotter, J. Phys. A **42**, 153001 (2009).
[20] W. D. Heiss, J. Phys. A **45**, 444016 (2012).
[21] M. Berry, Czech. J. Phys. **54**, 1039 (2004).
[22] V. M. Vyas and D. Roy, Phys. Rev. B **103**, 075441 (2021).
[23] R. Nehra and D. Roy, Phys. Rev. B **105**, 195407 (2022).
[24] H. Shen, B. Zhen, and L. Fu, Phys. Rev. Lett. **120**, 146402 (2018).
[25] W. P. Su, J. R. Schrieffer, and A. J. Heeger, Phys. Rev. Lett. **42**, 1698 (1979).
[26] J. Asbóth, L. Oroszlány, and A. Pályi, *A Short Course on Topological Insulators: Band Structure and Edge States in One and Two Dimensions*, Lecture Notes in Physics (Springer, Switzerland, 2016).
[27] C. Yin, H. Jiang, L. Li, R. Lü, and S. Chen, Phys. Rev. A **97**, 052115 (2018).
[28] E. J. Bergholtz, J. C. Budich, and F. K. Kunst, Rev. Mod. Phys. **93**, 015005 (2021).
[29] S. Rufo, N. Lopes, M. A. Continentino, and M. A. R. Griffith, Phys. Rev. B **100**, 195432 (2019).
[30] *Strongly Coupled Field Theories for Condensed Matter and Quantum Information Theory*, edited by A. Ferraz, K. S. Gupta, G. W. Semenoff, and P. Sodano, Springer Proceedings in Physics Vol. 239 (Springer, Cham, 2020).
[31] S. Rufo, M. Griffith, N. Lopes, and M. A. Continentino, Sci. Rep. **11**, 22524 (2021).
[32] R. Arouca, C. H. Lee, and C. Morais Smith, Phys. Rev. B **102**, 245145 (2020).
[33] G. Sun, J.-C. Tang, and S.-P. Kou, Front. Phys. **17**, 33502 (2022).
[34] X.-X. Bao, G.-F. Guo, X.-P. Du, H.-Q. Gu, and L. Tan, J. Phys.: Condens. Matter **33**, 185401 (2021).
[35] F. K. Kunst, E. Edvardsson, J. C. Budich, and E. J. Bergholtz, Phys. Rev. Lett. **121**, 026808 (2018).
[36] P. Comaron, V. Shahnazaryan, W. Brzezicki, T. Hyart, and M. Matuszewski, Phys. Rev. Res. **2**, 022051(R) (2020).
[37] S. Rahul and S. Sarkar, Sci. Rep. **12**, 6993 (2022).
[38] S. Yao and Z. Wang, Phys. Rev. Lett. **121**, 086803 (2018).
[39] C. H. Lee and R. Thomale, Phys. Rev. B **99**, 201103(R) (2019).
[40] M. A. Griffith and M. A. Continentino, Phys. Rev. E **97**, 012107 (2018).
[41] F. Sun and J. Ye, Phys. Rev. B **96**, 035113 (2017).
[42] S. Kempkes, A. Quelle, and C. M. Smith, Sci. Rep. **6**, 38530 (2016).
[43] A. Quelle, E. Cobanera, and C. M. Smith, Phys. Rev. B **94**, 075133 (2016).
[44] A. Mostafazadeh, J. Math. Phys. **43**, 3944 (2002).
[45] A. P. Schnyder, S. Ryu, A. Furusaki, and A. W. W. Ludwig, Phys. Rev. B **78**, 195125 (2008).
[46] A. Altland and M. R. Zirnbauer, Phys. Rev. B **55**, 1142 (1997).
[47] K. Kawabata, T. Bessho, and M. Sato, Phys. Rev. Lett. **123**, 066405 (2019).
[48] C. Wang and X. R. Wang, Phys. Rev. B **101**, 165114 (2020).